Temperature and Pressure Dependence of the Multichannel Rate Coefficients for the CH_3 + OH System

R. De Avillez Pereira, D. L. Baulch, M. J. Pilling,* S. H. Robertson, and G. Zeng

School of Chemistry, University of Leeds, Leeds LS2 9JT, U.K.

Received: July 2, 1997; In Final Form: October 7, 1997[⊗]

Laser flash photolysis measurements on the kinetics of the title system in a He bath gas are reported for the temperatures 290, 473, and 700 K and a pressure range of 7.6−678 Torr. CH_3 and OH radicals were generated simultaneously by 193 nm photolysis of acetone containing traces of water, with CH_3 in large excess. The course of reaction was followed by monitoring the concentration of OH using laser-induced fluorescence (LIF), while CH_3 was monitored by absorption at 216.4 nm. The experimental data were analyzed in the first instance by a simple model based on the decay of OH and CH_3, which was verified by more comprehensive numerical simulations. Further analysis of the data, using a combined master equation/inverse Laplace transform/RRKM procedure, yielded estimates of the association rate coefficient of CH_3 and OH ($k_1^\infty = (8.0 \pm 0.3) \times 10^{-11}$ (T/300 K$^{-0.79\pm0.09}$ cm^3 molecule^{-1} s^{-1}) and for the enthalpy change for the CH_3 + OH → $^1CH_2$ + H_2O channel ($\Delta H_0^\ominus = 1.6 \pm 2.0$ kJ mol^{-1}). Pressure-dependent rate coefficients for the various channels are also calculated and parameters for a modified Troe representation determined.

1. Introduction

The abundance of CH_3 and OH radicals in flames is such that an understanding of their reactions, particularly with each other, is crucial to the description of hydrocarbon combustion. The reaction of CH_3 and OH to give CH_3OH is an important sink for both of these radicals but is by no means the only channel by which they can react:

$$CH_3 + OH \rightarrow CH_3OH \quad \text{(R1.2)}$$

$$\rightarrow {}^1CH_2 + H_2O \quad \text{(R1.3)}$$

$$\rightarrow CH_3O + H \quad \text{(R1.4)}$$

$$\rightarrow CH_2OH + H \quad \text{(R1.5)}$$

$$\rightarrow CH_2O + H_2 \quad \text{(R1.6)}$$

$$\rightarrow HCOH + H_2 \quad \text{(R1.7)}$$

The channels, together with estimates of their threshold energies,[1,2] relative to the zero-point energy of CH_3OH, are shown in Figure 1. Many of the parameters given in Figure 1 are subject to debate, particularly the threshold of channel 3. An important question is whether it is this channel, or stabilization, that is the main exit route for the energized CH_3OH complex and how the channel efficiencies depend on temperature and bath gas concentration. Dean and Westmoreland[3] have performed calculations that suggest that the stabilization channel is the most significant at "normal pressures" and not too high a temperature. On the other hand Pilling and co-workers[4] have proposed a model that suggests that channel 3 is the dominant exit channel under conditions appropriate to combustion. This has important consequence for the flame speed, as described by Oser et al.[5] The importance of channel 3 depends sensitively on the energy asymptote for this channel.

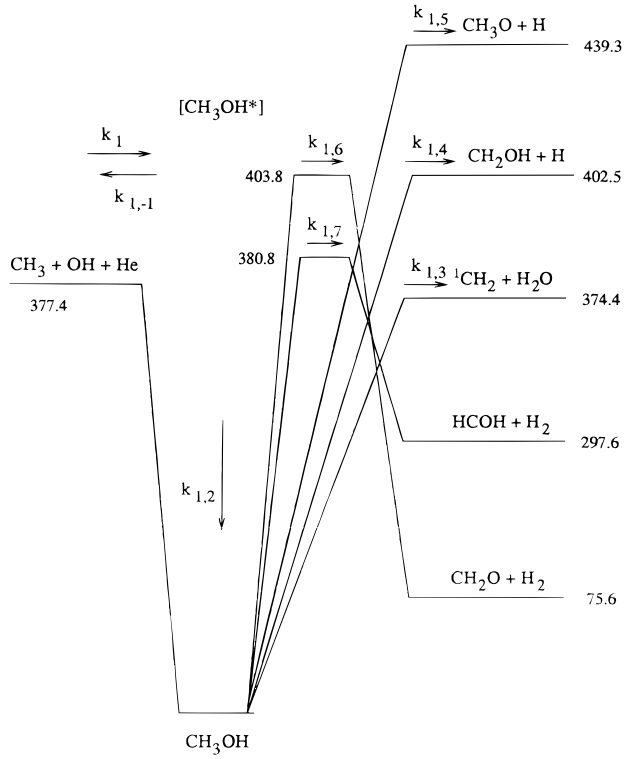

Figure 1. Channel energies for the multichannel reaction CH_3 + OH → products. Threshold energies of channels 1, 3−5 are taken from the Sandia database.[1] Channels 6 and 7 are taken from the calculation of Harding et al.[2] Energies are given in kJ mol^{-1}.

CH_3 + OH has been examined experimentally by a number of workers:

Hochanadel et al.[6] used laser photolysis of water to generate OH radicals from an excess of water vapor. H abstraction by OH from CH_4 was used to generate CH_3 which then went on to react via an association reaction with OH. The methyl radical concentration was monitored by time-resolved absorption at 216.4 nm, and the decay profiles were fitted to an 11-reaction

† Present address: Molecular Simulations Ltd., 240/250 The Quorum, Barnwell Road, Cambridge CB5 8RE, U.K.

⊗ Abstract published in *Advance ACS Abstracts,* November 15, 1997.

S1089-5639(97)02140-3 CCC: $14.00

mechanism. Their estimated value for the rate coefficient at 300 K and 750 Torr was $(9.2 \pm 4.6) \times 10^{-11}$ cm^3 molecule^{-1} s^{-1}.

Anastasi et al.[7] used pulse radiolysis to generate F atoms from SF_6 which then reacted with CH_4 and H_2O to yield the required reactants. The methyl radical concentration was again monitored by absorption at 216.4 nm. The rate coefficient at a temperature of 294 K and and a pressure of argon bath gas of 940 Torr was $(9.3 \pm 1.3) \times 10^{-11}$ cm^3 molecule^{-1} s^{-1} in good agreement with that of Hochanadel et al.[6]

Fagerström et al.[8] also used pulse radiolysis of $SF_6/CH_4/H_2O$ mixtures and CH_3 absorption at 216.4 nm. A pressure dependence of the decay of CH_3 radicals was observed and modeling of the data yielded a temperature-dependent high-pressure rate coefficient of $(15 \pm 1.5) \times 10^{-11}$ $(T/300\ \mathrm{K})^{0.1}$ cm^3 molecule^{-1} s^{-1}.

Laszlo et al.,[9,37] using flash photolysis of acetone and N_2O/H_2, coupled with detection by absorption and resonance fluorescence, obtained a the rate coefficient of $8.0(\pm 1.6) \times 10^{-11}$ cm^3 molecule^{-1} s^{-1} at a temperature of 300 K and for a pressure range of 34−350 Torr. There was no observed pressure dependence over the measured pressure range.

Bott et al.[10] measured the reaction at the higher temperature of 1200 K and at a pressure of 760 Torr behind reflected shock waves in argon. The source for both radicals was *tert*−butylhydroperoxide ($(CH_3)_3COOH$) which sequentially dissociates in the shock. The decay of OH was monitored by UV absorption at 309 nm. The rate coefficient was obtained by fitting the absorption profile to that generated from a 42-reaction mechanism. The stabilization channel was suggested to be the most important, accounting for 75% of the decay. The overall association rate coefficient was estimated as $(1.8 \pm 0.5) \times 10^{-11}$ cm^3 molecule^{-1} s^{-1}.

The most extensive work has been carried by Grotheer and co-workers.[5,11,12] In an early study[5] they examined the reaction using a flow technique in which excess OH was mixed with CH_3 in a flow tube. The decay of $[CH_3]$ was monitored using mass spectroscopy. An excess of OH was used to minimize the difficulties introduced by the methyl radical self-reaction and to create a situation that approached pseudo-first-order kinetics. It was however recognized by these workers that the complications of side reactions were such that computer modeling was required to analyse the results. The OH and CH_3 radicals were initially generated by the following reactions

$$H + NO_2 \rightarrow OH + NO \qquad \text{(R2)}$$

$$CH_4 + F \rightarrow CH_3 + HF \qquad \text{(R3)}$$

using H and F atoms generated in a microwave discharge. Typical concentrations were of the order $[CH_3] = 10^{11}$ molecule cm^{-3} and $[OH] = 10^{12}$ molecule cm^{-3}. One of the difficulties that was encountered was that, because of the presence of excess of H_2 used in generating H, the fraction of excited CH_3OH exiting through channel 3 could not be determined because the methylene formed reacted very rapidly to regenerate methyl radicals via the reaction

$$^1CH_2 + H_2 \rightarrow CH_3 + H \qquad \text{(R4)}$$

To overcome these problems, OD radicals, obtained from the reaction of F atoms with D_2O, were used instead and HDO monitored. It was found that reaction through channel 3 was slow compared with stabilization for the temperatures studied, and it was proposed that the threshold of channel 3 be revised from 0.1 to 7.5 kJ mol^{-1} above the threshold of the entrance channel, i.e., of $CH_3 + OH$. These workers concluded that stabilization was probably the dominant channel at the temperatures (300 and 480 K) and pressures (0.225−6.825 Torr) used. The overall rate coefficient was found to be pressure-dependent with a high-pressure association rate coefficient of 1.7×10^{-10} cm^3 molecule^{-1} s^{-1}, independent of temperature, although the measurements were made some way from the limit.

In a later paper[11] this work was extended to 700 K. Particular attention was focused on channels 6 and 7; it was concluded that at this higher temperature channel 7, but not channel 6, makes a significant contribution to the decay of the methanol complex. In these experiments OH radicals were generated by the action of F on H_2O. The excess of water required again prevented channel 3 from being assessed because of significant back reaction leading to very rapid establishment of an equilibrium for this channel. When D_2O was used however a 37% increase in the decay of $[CH_3]$ was found, presumably attributable to channel 3.

Hughes et al.[13] used laser flash photolysis to investigate the reaction at 290 K. Instead of excess OH, an excess of CH_3 was used. The concentration of CH_3 was monitored by absorption spectroscopy and that of the OH by laser-induced fluorescence. There are obvious difficulties in using excess of CH_3, because recombination dominates the CH_3 decay and it was necessary to monitor the time dependence of both radicals. They obtained only a weak pressure dependence over the range 7−700 Torr, with $k_1^\infty = (7.6 \pm 0.8) \times 10^{-11}$ cm^3 molecule^{-1} s^{-1}. The same method is used in the present work. The main objectives are determinations of the temperature dependence of k_1^∞, and assessment and parametrization of the channel rate coefficients, with an estimate of the threshold energy for channel 3.

Jordan et al.[14] have investigated the association channel theoretically. They performed canonical variational transition state theory calculations using an extended Gorin model in which the interaction between fragments was accounted for by addition of a simple hindered rotor potential. The values obtained for the limiting high-pressure association rate coefficient are fitted by the expression 17.2×10^{-11} $(T/300\ \mathrm{K})^{0.27}$ cm^3 molecule^{-1} s^{-1} indicating a weak, positive temperature dependence.

The structure of the paper is as follows: In section 2 the experimental technique is described and the photolysis processes used to generate the radicals are discussed in section 3. In section 4 the methods used to extract rate coefficients from experimental data are discussed and the experimental rate coefficients are presented. The multichannel nature of this reaction makes it a theoretically challenging system, and in section 5 the results are analyzed using methods based on the master equation approach and kinetic parameters are extracted. Concluding remarks are gathered in section 6.

2. Experimental Section

The experimental apparatus and procedure have been described previously,[13,15] and so only a short account is given here. The unfocused 193 nm output of a Lambda Physik LPX-100 laser was directed into a stainless steel reaction cell containing the precursors. CH_3 was monitored by UV absorption spectroscopy with a path length of 2.82 cm; light from an XBO-150 Wotan Xenon arc lamp was passed through the reaction cell and onto a Spex Czerny-Turner model 1870 0.5 m

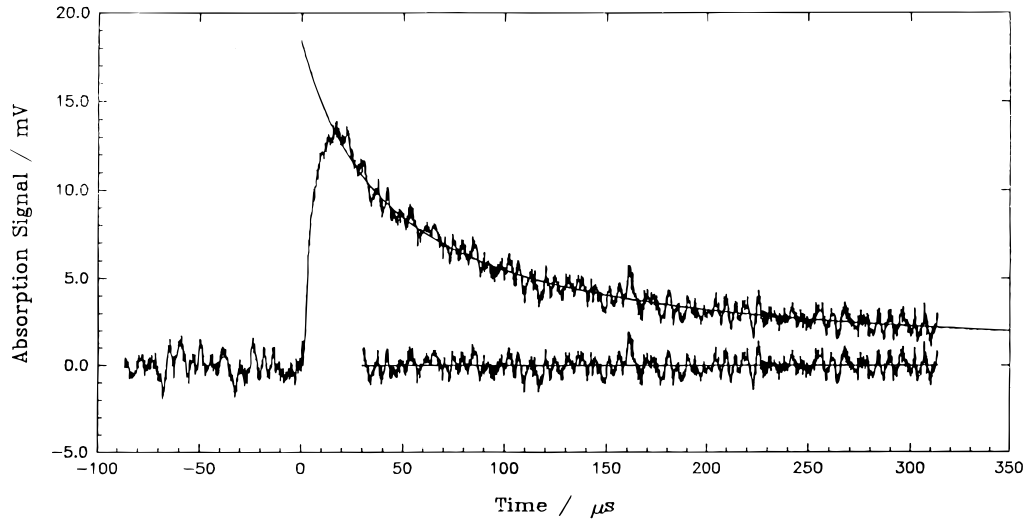

Figure 2. CH_3 radical decay monitored by UV-absorption at 213.36 nm and fitted to second-order rate at 8 Torr and 473 K. $[CH_3]_0 = 2.9 \times 10^{14}$ molecule cm^{-3}, $k_{rec} = 4.3 \times 10^{-11}$ cm^3 $molecule^{-1}$ s^{-1}.

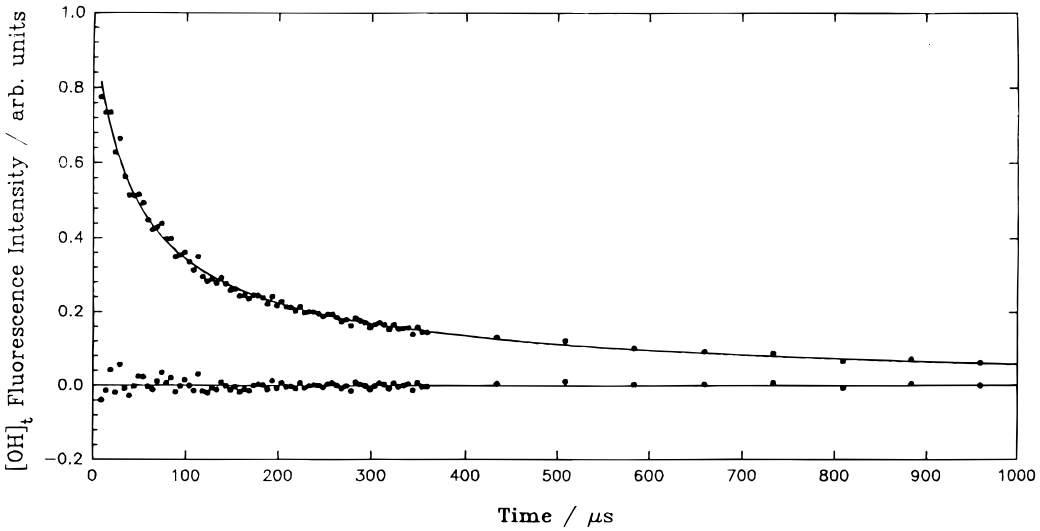

Figure 3. Typical LIF decay trace and residuals for OH radical: $A^2\Sigma^+ \rightarrow X^2\Pi$ transition near 308 nm.

monochromator, with a 0.6 nm band-pass, where the wavelength of 216.36 nm was selected, and monitored by a photomultiplier.

OH was monitored by laser-induced fluorescence (LIF). The frequency doubled output of a Nd-YAG pumped Spectron SL400 dye laser was tuned to 282.240 nm, the wavelength of the transition $A^2\Sigma^+(v'' = 1, K'' = 3) \leftarrow X^2\Pi(v' = 0, K' = 3)$. Fluorescence corresponding to the $A^2\Sigma^+(v'' = 0, \rightarrow X^2\Pi(v'' = 0)$ transition was collected along an axis orthogonal to both the photolysis and pump beams and focused on to a Thorn-EMI type 9813QB photomultiplier tube. Figures 2 and 3 show typical decay profiles for CH_3 and OH.

Gases were supplied with the following purities: He (BOC CP grade) 99.999%, H_2 (BOC CP grade) 99.999%, acetone (Aristar grade) 99.8%. The acetone was dried by repeatedly pumping samples in freeze−thaw cycles through a finely ground, dense column of anhydrous calcium chloride previously degassed. Residual H_2O cannot be removed by this process and is responsible for the generation of OH radicals during acetone photolysis, the most likely mechanism being a two-photon process.

3. Photolysis Processes

CH_3 was generated from the photolysis of acetone at 193 nm. This process has been examined in detail by Lightfoot et al.[16] who showed that the main photolysis channels are

$$(CH_3)_2CO \rightarrow 2CH_3 + CO \qquad \text{(R5.A)}$$

$$\rightarrow CH_2COCH_3 + H \qquad \text{(R5.B)}$$

$$\rightarrow CH_4 + CH_2O \qquad \text{(R5.C)}$$

with $\phi_A = 0.95$, $\phi_B = 0.03$, and $\phi_C = 0.02$ at 300 K, with a slight but negligible temperature dependence. In addition, CH_3 is photolyzed in the laser pulse

$$CH_3 \rightarrow CH_2 + H \qquad \text{(R6)}$$

CH_2 could be formed in either singlet, $^1CH_2$, or triplet, $^3CH_2$, states but, under the pressure conditions studied here, the singlet is rapidly deactivated so that only $^3CH_2$ is considered in the following analysis. Lightfoot et al.[16] showed that,

$$[^3CH_2]_0 = (0.31 \pm 0.21)\, F[\,CH_3]_0^{\,P} \qquad (1)$$

where F is the fractional photolysis

$$F = \frac{[CH_3]_0^{\,0}}{2\phi_A[(CH_3)_2CO]} \qquad (2)$$

and $[CH_3]_0^0 = [CH_3]_0^P - [^3CH_2]_0$ and the subscript refers to zero time, i.e. immediately after the laser pulse.

Thus the secondary radical yield increases as the laser intensity, and hence the fractional photolysis, increases. This process was encountered in the investigation by Brouard et al.[15] of the reaction $CH_3 + H$. It was particularly problematic, because the reaction between CH_3 and $^3CH_2$ generates H at concentrations comparable with that produced by photolysis if F is is too large. Accordingly they found it necessary to keep the laser intensity, and therefore $^3CH_2$, small. No such problem occurs with the present system, so that higher values for $[CH_3]_0$ can be employed with a consequent improvement in the signal to noise ratio. The contributions from secondary reactions are considered in detail below.

In the initial study of $CH_3 + OH$ (ref 13), OH was generated by photolysis of HNO_3. This introduces additional uncertainties arising from radical reactions with NO_2. Although simulations demonstrated that the effects on k_1 are <3%, it was decided to avoid this complication in the present study, when it was found that adequate concentrations of OH could be generated from residual water vapor. It is likely that this proceeds via a 2-photon process, probably generating OH $A^2\Sigma^+$ which relaxes either by collisional quenching or fluorescence on times short compared with the target reaction times.

$[OH]_0$ was approximately calibrated using 193 nm photolysis of N_2O/H_2/He mixtures, cross-correlating the signals with $[CH_3]_0$ from acetone photolysis. These experiments placed an upper limit of 10^{12} molecule cm^{-3} on $[OH]_0$. This source of [OH] was also used to determine the rate constant for diffusive loss of OH from the monitoring zone.

4. Data Analysis

The analysis of the accumulated experimental data is complicated by a number of features, not least being that, as the reaction of principal interest is between differing species, there must necessarily be competition from the the self-reactions of both species. Indeed, the concentration of methyl radicals generated is far in excess of that of the OH radicals and so methyl radical association

$$2CH_3 \rightarrow C_2H_6 \qquad \text{(R7)}$$

is the principal decay path of this reactant. (The photolysis fraction of CH_3 produced from acetone at 193 nm is between 10−30% which, for an initial acetone concentration of $(1-3) \times 10^{15}$ molecules cm^{-3}, gives $[CH_3] \geq 1 \times 10^{14}$ molecule cm^{-3}, with $[OH] < 1 \times 10^{12}$ molecule cm^{-3}.) $[CH_3]$ is given as a function of time by

$$[CH_3] = \frac{[CH_3]_0}{1 + 2k_7[CH_3]_0 t} \qquad (3)$$

Clearly, the value of $[CH_3]$ at any given time is dependent on $[CH_3]_0$, the initial concentration of radicals, and k_7, the rate coefficient for radical recombination. Because of their crucial importance to the analysis of the data we examine the factors that affect the accuracy with which $[CH_3]_0$ and k_7 are determined.

$[CH_3]$ was determined by absorption spectroscopy, and its absorption has been shown to follow a simple Beer−Lambert relation[17]. Thus

$$\Delta I(t)/I_0 = 1 - \exp\left(-\frac{\sigma(T) l [CH_3]_0}{1 + 2k_7[CH_3]_0 t}\right) \qquad (4)$$

where $\Delta I(t)$ is the change in absorption intensity, σ is the absorption cross section, and l is the path length. This expression was fitted to the absorption profiles using the Levenberg−Marquardt algorithm[18] allowing $[CH_3]_0$ and k_7 to float. Initial estimates of the parameters were determined without weighting. The squared residuals were then fitted to a cubic which was used to obtain estimates of the weights for each point. The fit was then repeated with these weights, and the parameters were found to change by less than 1% in all cases. The nature of this fit precludes an estimate of the goodness-of-fit. Estimates of the variance in the parameter values can be obtained in the usual way, i.e. as the diagonal elements of the curvature matrix of the fit, and will be denoted $\sigma^2_{k,\text{signal}}$ for k_7 and $\sigma^2_{[CH_3]_0,\text{signal}}$ for $[CH_3]_0$.

In addition to the signal errors just described there are errors introduced by the uncertainties in the initial intensity I_0 and the absorption cross section $\sigma(T)$. The uncertainty of I_0 is estimated to be less than 2% and corresponds roughly to the change in intensity before and after averaging over 1000 laser shots. The absorption cross section of the methyl radical was taken to be that calculated by Macpherson et al.[17]

$$\sigma(T) = (7.58 - 1.290 \times 10^{-2}\,(T/\text{K}) + 7.28 \times 10^{-6}\,(T/\text{K})^2) 10^{-17}\ \text{cm}^2/\text{molecule} \qquad (5)$$

using experimental data, with extrapolations above 537 K based on the calculations of Quack[19] and Ashfold[20], and has an estimated error of ±5%. These errors together with the signal errors were then propagated in the usual way

$$\sigma_k^2 = \sigma_{k,\text{signal}}^2 + \sigma_{I_0}^2\left(\frac{\partial k_7}{\partial I_0}\right)^2 + \sigma_{\sigma(T)}^2\left(\frac{\partial k_7}{\partial \sigma(T)}\right)^2 \qquad (6)$$

$$\sigma_{[CH3]_0}^2 = \sigma_{[CH3]_0,\text{signal}}^2 + \sigma_{I_0}^2\left(\frac{\partial [CH_3]_0}{\partial I_0}\right)^2 + \sigma_{\sigma(T)}^2\left(\frac{\partial [CH_3]_0}{\partial \sigma(\text{T})}\right)^2 \qquad (7)$$

where σ_{signal} refers to the estimate arising purely from a nonlinear least squares fit to the decay profile. These estimates of σ represent the internal error[21] of k_7 and $[CH_3]_0$. External error estimates are calculated, e.g., for k_7, as

$$(\sigma_k)_{\text{ext}} = \left(\frac{\sum_i (k_i - \bar{k})^2}{(n-1)}\right)^{1/2} \qquad (8)$$

where $\bar{k}$ is the sample mean. In the absence of systematic error the ratio of internal to external error should approach unity. In the present case there were significant deviations of more than a factor of factor of 2.

Additional sources of error include:

(i) Vibrational relaxation. Methyl radicals are produced in excited vibrational states, which has consequences for monitoring them by absorption spectroscopy as well as for their rate of reaction. The time scale for relaxation was established by monitoring the rise time of vibrational ground state. A maximum time of 30 μs was obtained under the lower pressure conditions studied here. More detailed, experiments have been conducted with Ar as the diluent giving similar results.[17] Data collected between 0 and 30 μs were thus omitted from the fit.

(ii) Secondary reactions. As discussed above, H is produced directly by photolysis of acetone and with CH_2 from the secondary photolysis of CH_3. Thus the yield of H and CH_2 increase with laser energy, i.e., with the fractional photolysis of acetone. Both of these reactants have the potential to interfere with methyl recombination kinetics via the reactions

$$CH_3 + H \rightarrow CH_4 \qquad \text{(R8)}$$

and

$$CH_3 + 3CH_2 \rightarrow C_2H_4 + H \qquad (R9)$$

The experiments were conducted with $[H]_0/[CH_3]_0$ between 0.02 and 0.06. A slight dependence of k_7 on this ratio was found, suggesting an overestimate in k_7 of ≈5%. The major contributor to the error is reaction (R8) and the largest error occurs at high pressure, because $k_8/2k_7$ increases with pressure. This question is returned to below in the discussion of numerical simulations of the reaction system.

(iii) Concentration gradient. Every effort was taken to ensure that any concentration gradients in the irradiated and monitored volumes were minimal, primarily because the CH_3 measurement was made over an extended volume, while that for OH was essentially at a point. Only the central more homogeneous section of the exciter laser beam was employed. Previous simulations have demonstrated that the errors introduced by small spatial inhomogeneities, in multiple measurements of second-order reactions, are minimal.[22]

It was not possible to ascertain the exact source of the systematic error and thereby eliminate it from the data; the larger of the two error estimates are consequently reported here (a practice advocated by Cvetanović et al.[21]) and used in the master equation analysis.

Having obtained estimates of k_7 and $[CH_3]_0$ for all of the experimental conditions it is now possible to analyze the decay of OH as monitored by LIF. The basis of this analysis is the rate equation

$$-\frac{d[OH]}{dt} = k_1[CH_3](t)\,[OH](t) + k_{10}[Ac][OH](t) + k_{diff}[OH](t) \qquad (9)$$

The first term on the right-hand side accounts for the reaction of principal interest in this study, k_1 being the required rate coefficient. The second term accounts for the reaction of OH radicals with the excess acetone

$$(CH_3)_2CO + OH \rightarrow CH_3COCH_2 + H_2O \qquad (R10)$$

and has rate coefficient k_{10}. Acetone is in sufficient excess for this reaction to be considered first order. The rate coefficient k_{10} has been measured by a number of workers. In this study the recommended expression of Wallington et al.,[23] $k_{10} = (1.7 \pm 0.4) \times 10^{-12} \exp(-(600 \pm 75)/T)$cm^3 molecule^{-1} s^{-1}, was used and yields a value of 2.1×10^{-13} cm^3 molecule^{-1} s^{-1} at 290 K. The third term accounts for the diffusion of the OH radicals out of the observation region.

Substitution of eq 3 for $[CH_3]$ in eq 9 followed by integration yields

$$\frac{[OH](t)}{[OH]_0} = (1 + 2k_7[CH_3]_0 t)^{-\beta} \exp(-k't) \qquad (10)$$

where $k' = k_{10}[Ac](0) + k_{diff}$ and $\beta = k_1/2k_7$, provided that $k_1[CH_3][OH] \ll 2k_7[CH_3]_2$ and $[Ac](t) = [Ac](0)$. The averaged fluorescence intensity, I_f, is proportional to the OH radical concentration, and the decay profiles were fitted to

$$I_f(t) = I_f(0)(1 + 2k_7[CH_3]_0 t)^{-\beta} \exp(-k't) \qquad (11)$$

using the same Levenberg−Marquardt[18] procedure as outlined earlier. The parameters β and k' were allowed to float and the optimum fit was taken as the parameter set that minimized χ^2. The reaction with methyl radicals is by far the most important OH decay channel, and the fit of the decay was, therefore, dominated by the reciprocal term, with the exponential term functioning as a time-dependent correction factor. The initial concentration of acetone was determined from its partial pressure, and the determination of $[CH_3]_0$ was described earlier. The values of the rate coefficient k_1 obtained are recorded in Table 1.

TABLE 1: Experimental Results for k_1 and k_7[a]

temp/K	pressure helium/Torr	10^{11} k_1/cm^3 molecule^{-1} s^{-1}	10^{11} k_7/cm^3 molecule^{-1} s^{-1}	no. of determinations
290.0	7.6	8.49 ± 1.16	5.19 ± 0.52	14
290.0	15	7.70 ± 1.32	5.79 ± 0.73	18
290.0	46	7.54 ± 0.88	6.09 ± 0.77	24
290.0	100	7.51 ± 1.14	6.46 ± 0.67	17
290.0	474	7.46 ± 0.75	6.07 ± 0.87	5
290.0	667	7.70 ± 0.90	6.08 ± 0.70	11
290.0	678	7.38 ± 0.74	6.27 ± 0.73	11
473.0	8.0	4.80 ± 1.08	3.63 ± 0.67	10
473.0	11	4.67 ± 1.42	3.76 ± 0.88	11
473.0	17	5.11 ± 0.77	4.00 ± 0.36	6
473.0	46	5.34 ± 0.80	4.62 ± 0.82	4
473.0	74	5.34 ± 1.10	4.36 ± 0.42	12
473.0	98	5.17 ± 0.78	4.80 ± 0.67	4
473.0	111	5.40 ± 0.99	4.71 ± 0.32	6
473.0	192	5.49 ± 0.82	5.21 ± 1.18	6
473.0	239	5.98 ± 1.73	4.94 ± 0.88	3
473.0	281	5.02 ± 0.75	4.91 ± 0.31	5
473.0	318	6.29 ± 1.48	4.68 ± 0.62	11
473.0	415	5.89 ± 1.35	4.72 ± 0.45	11
473.0	570	5.79 ± 0.87	5.26 ± 0.87	11
700.0	20	2.44 ± 0.61	2.14 ± 0.34	11
700.0	41	2.76 ± 0.83	2.87 ± 0.79	14
700.0	95	2.72 ± 0.68	2.95 ± 0.73	6
700.0	142	2.99 ± 0.73	3.12 ± 0.65	5
700.0	186	3.19 ± 1.48	3.28 ± 0.80	28
700.0	246	3.36 ± 1.17	3.26 ± 0.46	9
700.0	284	3.91 ± 0.98	3.46 ± 0.29	6
700.0	329	3.89 ± 0.97	3.53 ± 0.57	4
700.0	385	3.33 ± 0.83	3.69 ± 0.45	6
700.0	429	4.11 ± 1.46	3.50 ± 0.46	5
700.0	478	3.96 ± 0.99	3.69 ± 0.52	7
700.0	594	3.59 ± 1.22	3.48 ± 0.74	8

[a] Decay profiles were fitted using the analytic representations for $[CH_3]$ (eq 4) and [OH] (eq 11). The error limits represent ±2 standard deviations, determined from the external estimate σ_{ext}.

The principal sources of error in the measurement of k_1 arise from errors in k_7 and $[CH_3]_0$ and, since these parameters were not measured independently, their covariance. The errors in these quantities and those due to the signal were propagated and estimates of the variance in k_1 were obtained from

$$\sigma_{k_1}^2 = \sigma_{k_1,signal}^2 + \sigma_{k_7}^2\left(\frac{\partial k_1}{\partial k_7}\right)^2 + \sigma_{[CH_3]_0}^2\left(\frac{\partial k_1}{\partial [CH_3]_0}\right)^2 + 2\rho(k_7,[CH_3]_0)\sigma_{k_7}\sigma_{[CH_3]_0}\left(\frac{\partial k_1}{\partial k_7}\right)\left(\frac{\partial k_1}{\partial [CH_3]_0}\right) \qquad (12)$$

where $\rho(k_7,[CH_3]_0)$ is the covariance of k_7 and $[CH_3]_0$ and was determined for each pressure and temperature from the absorption data. The contribution to the error from $\rho(k_7,[CH_3]_0)$ is very small, since the combined error from $[CH_3]_0$ and k_7 is ≈±10% (±2 standard deviations) under all conditions. Typically the total lower bound to the internal estimate of the error (±2 standard deviations) is ±10%, ±15%, and ±25%, at 290, 474, and 700 K respectively. A comparison between internal and external standard deviations shows that the errors given by eq 15 are consistent with an absence of systematic error.

Additional sources of error include:

(i) Assumption of pseudo-first-order conditions. Equation 11 only holds if pseudo-first-order conditions apply, and this in turn depends on the ratio $[CH_3]_0/[OH]_0$. Calculations show that the depletion of methyl radicals by reaction with OH

TABLE 2: Mechanism Used in the FACSIMILE Integration

	reaction	k/cm^3 molecule^{-1} s^{-1}	ref	$\Delta \log k$ (see ref 45)
R1	$CH_3 + OH + He \rightarrow$ products	k_1	this study	
R7	$CH_3 + CH_3 + He \rightarrow C_2H_6$	k_7	this study	
R8	$CH_3 + H \rightarrow CH_4$	$k^0 = 6.2 \times 10^{-29}(T/300\ K)^{-1.8}$	45	±0.2
		$k^\infty = 3.5 \times 10^{-10}$	45	±0.3
		$F_c = \exp(-0.45 - T/3231\ K)$	45	±0.1
R9	$CH_3 + {}^3CH_2 \rightarrow C_2H_4 + H$	7.0×10^{-11}	45	±0.3
R10	$OH + (CH_3)_2CO \rightarrow H_2O + CH_3COCH_2$	$1.7 \times 10^{-12} \exp(-600\ K/T)$	24	±0.2
R11	$CH_3 + CH_3COCH_2 \rightarrow CH_3COC_2H_5$	$k \approx k_7$	estmd	±0.5
R12	$OH + CH_3COCH_2 \rightarrow CH_3COCH_2OH$	5.0×10^{-11}	estmd	±0.5
R13	$OH + {}^3CH_2 \rightarrow CH_2O + H$	3.0×10^{-11}	47	±0.5
R14	$OH + CO \rightarrow H + CO_2$	$1.05 \times 10^{-17} T^{1.5} \exp(250\ K/T)$	45	±0.2
R15	$OH + H \rightarrow H_2O$	$4.3 \times 10^{-25} T^{2.6}$[He]	48	±0.3
R16	$2OH \rightarrow H_2O + O$	$2.5 \times 10^{-15} T^{1.14} \exp(50\ K/T)$	45	±0.2
R17	$OH + OH \rightarrow H_2O_2$	$k^\infty = 1.5 \times 10^{-11}(T/300\ K)^{-0.37}$	45	±0.5
		$k^0 = 8.0 \times 10^{-31}(T/300\ K)^{-0.76}$	45	±0.4
		$F_c = 0.5$	45	±0.2
R18	${}^3CH_2 + {}^3CH_2 \rightarrow C_2H_2 + 2H$	$2.0 \times 10^{-10} \exp(-400\ K/T)$	45	±0.5
R19	${}^3CH_2 + H \rightarrow CH + H_2$	$1.0 \times 10^{-10} \exp(-400\ K/T)$	45	±0.3
R20	$2CH_3COCH_2 \rightarrow C_6H_{10}O_2$	$k \approx k_7$	estmd	±0.5

TABLE 3: Comparison of 290 K Rate Coefficients Determined from Basic and FACSIMILE Models

	$10^{11} k_1$/cm^3 molecule^{-1} s^{-1}		$10^{11}\ k_7$/cm^3 molecule^{-1} s^{-1}	
pressure/Torr	Facsimile	eq 11	Facsimile	eq 4
7.8	8.3 (±1.1)	8.5 (±1.2)	4.8 (±0.6)	5.2 (±0.5)
15	7.9 (±1.3)	8.2 (±1.3)	4.8 (±0.7)	5.8 (±0.7)
46	7.3 (±0.9)	7.5 (±0.9)	5.0 (±0.6)	6.1 (±0.8)
100	6.8 (±0.8)	7.4 (±1.1)	5.8 (±0.8)	6.5 (±0.7)
474	7.3 (±0.9)	7.4 (±0.8)	5.5 (±0.4)	6.1 (±0.7)
667	7.6 (±0.9)	7.7 (±0.7)	5.4 (±0.8)	6.2 (±0.7)

radicals decreases the observed k_1 by 7% for a $[CH_3]_0[OH]_0$ ratio of 10 and by 1% for a ratio of 50. Since [OH] is estimated to be less than 10^{12} molecule cm^{-3} it follows that the error associated with this assumption is less than 1%.

(ii) The major potential source of systematic error derives from contributions to the decay of both CH_3 and OH by reaction with species other than those explicitly recognized in the analytic time dependencies presented above. The reactions which could contribute are listed in Table 2. The inclusion of such reactions renders the kinetic equations insoluble analytically, and recourse to numerical techniques is necessary. To assess the effects that secondary reactions introduce, and the sensitivity of k_1 and k_7 to these reactions, a more extensive model of the reaction system was compiled and integrated using FACSIMILE in an analysis of the data at 290 K. Some reactions, e.g., the association of OH radicals to give H_2O_2, have a negligible effect on the system, because the concentration of OH is so small, but are included for the sake of completeness. The parameters $[CH_3]_0$, k_1, k_7, and k_{10} were floated and their best fit values determined by integrating the model, calculating absorption and fluorescence intensities and comparing with experimental absolute $[CH_3]$ and relative OH intensities. The initial concentrations of CO, H, CH_2COCH_3, and ${}^3CH_2$ were linked to $[CH_3]_0$ via the results of Lightfoot et al.[16] and $[OH]_0$ was estimated, relative to $[CH_3]_0$, from the approximate N_2O photolysis experiments. The best fit parameters were judged to be those that minimized χ^2.

The results of the FACSIMILE integration are summarized in Table 3, which shows the rate coefficients k_1 and k_7 determined from both the simple model and the full numerical model, at 290 K and for each of the pressures considered. The concentration of OH was varied between 10^{11} and 10^{12} molecule cm^{-3} and both k_1 and k_7 were found to be independent of this variation. The differences in k_1 between the FACSIMILE and analytical results are very small, typically around 2%, and well within experimental error. Experimental confirmation was obtained by plotting the analytically derived k_1 values against fractional photolysis; there was no discernible correlation. Similar behavior was observed at 473 and 700 K. The recommended rate constants are those given in Table 1.

A somewhat greater effect was found for k_7 with decreases of ≈10−20% on full FACSIMILE analysis. The major contribution derives from $CH_3 + H$. In consequence, the rate coefficients given in Table 1 are likely to be slight over estimates of k_7. The error in $[CH_3]_0$ is small (<2%) and, as Table 3 shows, little error from k_7 is propagated through to k_1. The analytical procedure derives an effective second-order rate coefficient for CH_3 decay that provides an accurate representation for use in eq 9 over the whole of the OH decay.

The analytic and numerical data fitting procedures also allow estimates to be made of k_{10}. Use of eq 10, with separately measured values of k_{diff}, gave averaged values of 2.6×10^{-13}, 7.1×10^{-13}, and 1.3×10^{-12} cm^3 molecule^{-1} s^{-1} at 290, 473, and 700 K, respectively, while numerical integration gave 3.3×10^{-13} cm^3 molecule^{-1} s^{-1} at 290 K. Uncertainties were typically a factor of 2: the experiments are relatively insensitive to k_{10}. Within these error bounds, the results are consistent with the Arrhenius expressions recommended by Wallington et al.[23] which gives values of 2.1, 4.8, and 7.2×10^{-13} cm^3 molecule^{-1} s^{-1} at the three temperatures concerned. It should be emphasized that the exponential term makes a comparatively small contribution to the decay of OH.

5. Master Equation Analysis

The $CH_3 + OH$ reaction is an example of a system that proceeds through a strongly bound complex and has associated with it several other product channels—a so-called multichannel reaction. In the present case the number of accessible channels is seven, including collisional relaxation to the stable CH_3OH molecule and dissociation back through the input channel to give the reactants, as illustrated in Figure 1. Such systems are best analyzed in the context of unimolecular rate theory. The most widely used approach is that due to Troe and coworkers,[24−26] the basis of which is the Lindemann−Hinshelwood theory which is corrected for the effects of energy-dependent microcanonical rate coefficients and weak collisions by appending a number of factors to the original Lindemann−Hinshelwood formula. This approach is ideally applied to systems which are single-channel unimolecular decomposition or association reactions. Although this approach has been extended to multichannel reactions,[27] it has not been validated for such systems.

A more natural approach, in which incorporation of any number of reaction channels is straightforward, is afforded by

the master equation (ME) formalism. The energy of the adduct $X(\equiv CH_3OH)$ is divided into a contiguous set of intervals or grains. Each grain contains a bundle of rovibrational states to which are ascribed a common, averaged energy, E_i, and microcanonical rate coefficients for dissociation, k_i^n, where n refers to the reaction channel and can take the values 1, 3−7 (see Figure 1). The ME describes the evolution of the grain populations

$$\frac{\mathrm{d}}{\mathrm{d}t}\rho_i(t) = \omega\sum_j P_{ij}\rho_j(t) - \omega\rho_i(t) - \sum_n k_i^n\rho_i(t) + R_i \quad (13)$$

where R_i is the rate of population of $X(E_i)$ from CH_3 + OH, ω is the frequency of collisions between X and the bath gas, M, and P_{ij} is the probability of transfer of X from grain j to grain i on collision with M. An exponential down model[29] was assumed for P_{ij}, defined by the parameter $\alpha(=\langle\Delta E\rangle_{\mathrm{down}}^{-1})$. Upward transitions where determined by detailed balance. The details of the method of calculation are given in ref 28.

The rate of population, R_i, is given by detailed balance[29]

$$R_i = k_1^\infty[CH_3][OH]\eta_i = R'\eta_i \quad (14)$$

where k_1^∞ is the limiting high-pressure association rate coefficient and η_i is given by

$$\eta_i = \frac{k_i^1 f_i}{\sum_i k_i^1 f_i} \quad (15)$$

where f_i is the equilibrium Boltzmann distribution of $X(E_i)$. R_i is both time-dependent and nonlinear (because $[CH_3]$ varies with time). However, since $[CH_3] \gg [OH]$ the decay of CH_3 is unaffected by OH. Provided the reactants are maintained in a Boltzmann distribution, it is possible to utilize the master equation to model this system by incorporating an absorbing boundary, sufficiently below the lowest reaction threshold that collisional energization from that boundary is highly improbable, to simulate irreversible stabilization.[28]

The ME can be expressed in matrix form as

$$\frac{\mathrm{d}\boldsymbol{\rho}}{\mathrm{d}t} = \mathbf{M}\boldsymbol{\rho} + R'(t)\boldsymbol{\eta} \quad (16)$$

where $\boldsymbol{\rho}$ is a vector containing the grain populations, $\boldsymbol{\eta}$ is a vector containing the fractional rates defined in eq 14 and $\mathbf{M}$ is given by,

$$\mathbf{M} = \omega[\mathbf{P} - \mathbf{I}] - \sum_n \mathbf{K}^n \quad (17)$$

$\mathbf{P}$ being the collision matrix, $\mathbf{I}$ the unit matrix, and $\mathbf{K}^n$ a diagonal matrix with the sum of the microcanonical rate coefficients (averaged over each grain) for the n channels on the diagonal (note n is not an exponent).

The solution for this irreversible system is characterized by a fast transient period followed by a steady-state regime in which the shape of the population distribution remains constant. The steady-state solution can be obtained from eq 16, by setting the time derivative and all reactivation rates from the absorbing boundary to zero. The steady-state population distribution $\boldsymbol{g}$ can then be obtained by inversion of the truncated matrix.

$$\mathbf{g} = -R'(t)\,\mathbf{M}^{-1}\boldsymbol{\eta} \quad (18)$$

The observed rate of decay of OH can be derived from $\boldsymbol{g}$ by invoking mass conservation and noting that the sum of fluxes into each of the product channels, including stabilization, must equal the decay flux of the OH

$$R_{\mathrm{ob}} = k_1[CH_3][OH] \quad (19)$$

$$= \sum_i[\omega P_{c,i} + \sum_n k_i^n]g_i \quad (20)$$

where R_{ob} is the observed rate of association, k_1 is the observed rate coefficient for association, $\omega P_{c,i}$ is the rate of collisional transfer from the ith state to the absorbing boundary, and k_i^n is the rate coefficient for reaction from the ith state into product channel n. Combining eqs 18, 19, and 20 yields

$$k_1 = k_1^\infty\sum_i[\omega P_{c,i} + \sum_n k_i^n](\mathbf{M}^{-1}(-\boldsymbol{\eta}))_i \quad (21)$$

which was used in the fitting of experimental data and extracting of kinetic parameters from them.

The density of states of CH_3OH were calculated by using a combination of the Beyer−Swinehart algorithm[30,31] for the vibrational modes and a classical densities of states treatment for the rotational modes. CH_3OH has an internal rotational mode that couples with the external rotations and is best treated as a free rotor rather than a vibration. The classical treatment adopted by Seakins et al.[32] in their analysis of internal rotation of the isopropyl radical was employed. The combined rovibrational density of states was obtained by a convolution in the usual way.

The microcanonical rate coefficients were determined using either RRKM theory or inverse Laplace transformation (ILT). Channels 1,3−5 occur on type II potential energy surfaces, with no potential barrier. A variational approach must be employed to calculate k_i, and the model must properly account for the interaction of the angular modes of motion, which are important determinants of the microcanonical rate coefficients and their dependence on energy. The calculation of realistic rate coefficients is difficult and requires the use, for example, of the statistical adiabatic channel or flexible transition state models, which are computationally intensive and difficult to use in the analysis of experimental data. Accordingly, the ILT method, which directly links k_i to experimental association rate coefficients, was used for these channels. The details of the ILT technique have been described elsewhere[33]—in brief, canonical and microcanonical rate coefficient are related via a Laplace transform, and if an Arrhenius form of the canonical rate coefficient is available then the microcanonical rate coefficient can be obtained by taking the inverse transform. Often, as is the case for many of the channels for the present system, the association canonical rate coefficient is better characterized than the dissociation coefficient, mainly because its temperature dependence is much weaker. Davies et al.[33] exploited this observation in their formulation of the ILT technique. If the Arrhenius form for the association can be expressed as

$$k^\infty = A^\infty(T/T^\infty)^{n^\infty}\exp(-\beta E^\infty) \quad (22)$$

where $\beta = 1/kT$, such that $n^\infty > -1.5$, then the microcanonical rate coefficient is given by

$$k(\mathrm{E}) = \frac{A^\infty C'}{N(E)\,\Gamma(n^\infty + 1.5)}\int_0^{E-E^\infty-\Delta H_0^0} N_{\mathrm{p}}(x)[(E - E^\infty - \Delta H_0^0) - x]^{n^\infty+0.5}\,\mathrm{d}x \quad (23)$$

where $N(\cdot)$ is the density of states for the unimolecular reactant, $N_{\mathrm{p}}(\cdot)$ is the convoluted densities of states of the product species, ΔH_0^0 is the zero-point energy difference between the reactants

TABLE 4: Parameters Used To Estimate the Microcanonical Rate Coefficients of Each Channel

channel	reactants	$10^{11}k$/ cm^3 molecule^{-1} s^{-1}	ref
1	$CH_3 + OH$	$8.0(T/300\ K)^{-0.79}$	this study
3	$^1CH_2 + H_2O$	16	35, 36
4	$CH_2OH + H$	16	47
5	$CH_3O + H$	1.3	49, 50

and products, and $\Gamma(\cdot)$ is the Gamma function. C' is given by

$$C' = \left[\frac{2\pi M_A M_B}{h^2(M_A + M_B)}\right]^{3/2} \tag{24}$$

where M_A and M_B are the masses of the dissociation products.

The ILT method was used to estimate k_i^n for channels 1, 3−5. The association rate coefficients used for channels 3−5 are shown in Table 4. Note that the temperature dependence of k_n^∞ has not been determined for channels 3−5, and it was assumed that the limiting rate constants are independent of temperature. The parameters defining k_1^∞ are the target of the analysis and the form

$$k_1^\infty = A_1^\infty (T/300\ K)^{n^\infty} \tag{25}$$

was employed. The molecular parameters used in the ILT analysis are given in Appendix A.

Experimental data for channels 6 and 7 are more limited. However, there is a well-defined maximum in both cases, and the energies, geometries, and vibrational frequencies of the transition states have been calculated by Walch.[34] Accordingly, RRKM theory was used to calculate the microcanonical rate coefficients

$$k(E) = \frac{W(E)}{hN(E)} \tag{26}$$

where $W(E)$ is the sum of states at the transition state.

Having obtained estimates of the microcanonical rate coefficients, the fitting of data via eq 21 could now proceed. As with previous analyses, the fitting criterion was the minimization of χ^2, where χ^2 is defined as

$$\chi^2 = \sum_i (k_{exp,i} - k_{cal,i})^2/\sigma_i^2 \tag{27}$$

$k_{exp,i}$ being the experimentally determined values at various temperatures and pressures, $k_{cal,i}$ the corresponding values calculated using eq 21 and σ_i the estimates of the experimental error. χ^2 depends on the values of various kinetic parameters, and the best values of these parameters is deemed to be those which minimize χ^2. The minimization of χ^2 is difficult: clearly $k_{cal,i}$ is a very complex function of the parameters, and so a nonlinear least squares method is obligatory. Nonlinear methods rely on a knowledge of the derivatives of the function to be minimized with respect to the parameters, but here again the complexity of the function means there is little hope of obtaining analytic derivatives. Numerical derivatives can be obtained, but they are time consuming. For fitting and analysis purposes, it is most expedient to perform a simple grid search of the parameter space.

For the data reported here, the most important parameters were identified as the Arrhenius parameters A_1^∞ and n_1^∞ of channel 1 and the threshold energy of channel 3, $\Delta H_{0,3}^0$. In first instance, A_1^∞ and n_1^∞ were floated and fitted. $\Delta H_{0,3}^0$ was fixed at the value which was taken from the Sandia database[1]. $\langle\Delta E\rangle_{down}$ was fixed at 230 cm^{-1}. The errors reported in Table 1 were used to weight each datum point. The best fit values obtained were (±2 standard deviations):

$$A_1^\infty = (7.8 \pm 0.3) \times 10^{-11}\ \text{cm}^3\ \text{molecule}^{-1}\ \text{s}^{-1}$$

$$n_1^\infty = -0.81 \pm 0.09 \tag{28}$$

The ME calculations give overall rate constants which are independent of [M], in good agreement with experiment, for the threshold energy for channel 3 shown in Figure 1. Since this channel is exothermic, all states populated from $CH_3 + OH$ have $k_i^3 > 0$. At low pressures, reaction occurs primarily via channel 3 and at high pressures by stabilization. Under all conditions, dissociation to regenerate the reactants $CH_3 + OH$ is slow in comparison and $k_1 \approx k_1^\infty$. This conclusion is unaffected by modest increases in $\Delta H_{0,3}^0$. Calculations based on the threshold energy proposed by Grotheer and coworkers,[5,11,12] however, with channel 3 higher in energy that channel 1 by 7.5 kJ mol^{-1}, produces a significant increase in k_i^1/k_i^3, so that dissociation along channel 1 becomes significant and the rate constant falls off below k_1^∞ at lower pressures: a much higher value of $\langle\Delta E\rangle_{down}$ (>700 cm^{-1}) is needed to reproduce the experimental data. It is, however, difficult to determine a more precise value for $\Delta H_{0,3}^0$ on the basis of our experimental data.

A more precise location of the threshold energy for channel 3 can be obtained from an analysis of the experimental data of Hack et al.[35] for the reverse reaction

$$^1CH_2 + H_2O \rightarrow CH_3 + OH \qquad (R1.-3)$$

They obtained a rate constant for the overall reaction of $^1CH_2 + H_2O$, exclusive of stabilization to $^3CH_2$, of 1.6×10^{-10} cm^3 molecule^{-1} s^{-1}, with the OH channel accounting for 50−100%. Later measurements by Carstensen et al.[36] reveals that this channel contributes 50 ± 15% to the total reaction at the same conditions. If $\Delta H_{0,3}^0 \leq \Delta H_{0,1}^0$, then reverse dissociation, from the energized CH_3OH formed from $^1CH_2 + H_2O$ in the experiments of Hack et al.[35] may be significant, implying that the high-pressure limiting rate constant for channel 3, which is needed for the ILT calculations, is higher than that measured by Hack et al.[35] A modified form of the ME/ILT was set up, with $^1CH_2 + H_2O$ as the input channel. The channel efficiency in (R1.−3) was calculated, allowing $\Delta H_{0,3}^0$ and $k_{1,-3}^\infty$ to float.

An additional constraint was placed on the fit using recent data by Temps et al.[37] who detected $^3CH_2$ in studies of the $CH_3 + OH$ reaction. The inference is that $^3CH_2$ is formed by deactivation of $^1CH_2$ formed directly in reaction 1 (see below). They found that, at a pressure of 1 Torr at 296 K, (73 ± 16)% of the reaction leads to $^1CH_2$ formation. The parameters derived from the fit to the Hack/Carstensen[35,36] data for $^1CH_2 + H_2O$ were used to calculate the yield of $^1CH_2$ from $CH_3 + OH$, for comparison with the experimental measurements of Temps et al.[37] Together, these data provide a significant constraint on $\Delta H_{0,3}^0$. If it is too high, the yield of $^1CH_2$ from $CH_3 + OH$ falls below the experimental value. If it is too low, then an unphysically high value of $k_{1,-3}^\infty$ is needed to be compatible with the data of Carstensen et al.[36] The most satisfactory fits are obtained with

$$\Delta H_{0,3}^0 - \Delta H_{0,1}^0 = 1.6 \pm 2\ \text{kJ mol}^{-1}$$

$$k_{1,-3}^\infty = 2.5 \pm 10^{-10}\ \text{cm}^3\ \text{molecule}^{-1}\ \text{s}^{-1} \tag{29}$$

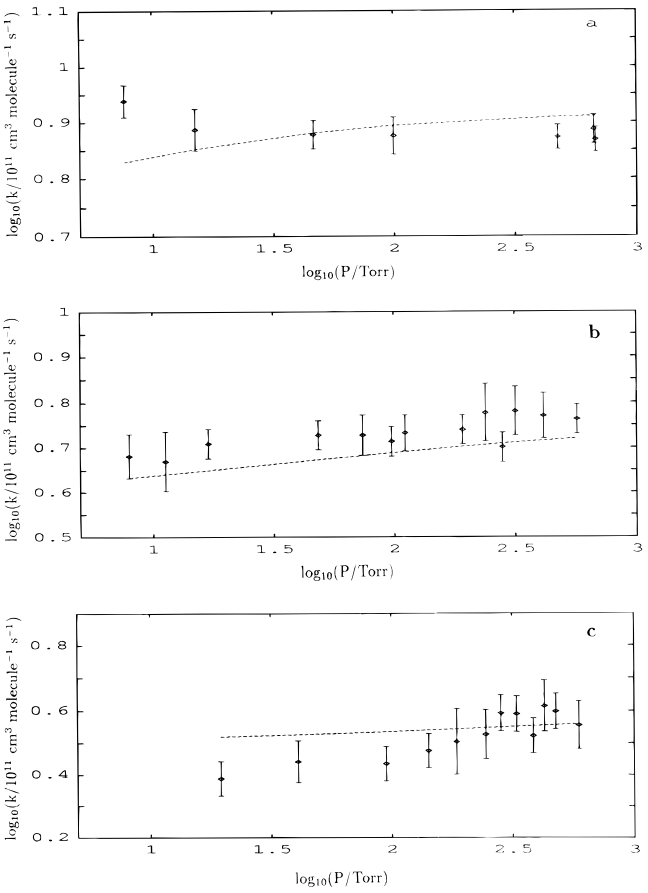

Figure 4. Experimental data of this work and best fit fall-off curves using the ME model: (a) 290 K, (b) 473 K, and (c) 700 K. The error bars represent $\pm 2\sigma$.

TABLE 5: Comparison of Calculated and Measured Rate Coefficients for the Conditions Reported by Fagerström et al.[8]

temperature/ K	pressure/ Torr	$10^{11}k_{cal}$/ cm^3 molecule^{-1} s^{-1}	10^{11} k_{exptl}/ cm^3 molecule^{-1} s^{-1}
298.0	63.8	7.9	9.6 ± 0.5
298.0	127.5	7.9	10.0 ± 0.5
298.0	375.0	8.0	12.1 ± 1.2
298.0	750.1	8.0	13.0 ± 1.3

The experimental data reported in this paper were then refitted using these values. The optimal fits for k_1^∞ were little affected

$$A_1^\infty = (8.0 \pm 0.3) \times 10^{-11} \text{ cm}^3 \text{ molecule}^{-1} \text{ s}^{-1}$$

$$n_1^\infty = -0.79 \pm 0.09 \qquad (30)$$

where the uncertainties refer to $\pm 2\sigma$. The data and the fits are shown in Figure 4. The goodness-of-fit was calculated to be 0.0839 from the χ^2 distribution.

6. Discussion

The enthalpies of formation ($\Delta H^0_{f,298}$) of the species involved in channels 1−6 are tabulated in Table 6, for the Sandia[1] and JANAF[38] databases.

The difference in reaction thresholds for channels 1 and 3, $\Delta H^0_{0,r}$, can be determined from these enthalpies of formation, together with the changes in enthalpies of formation between 0 and 298 K, calculated from the spectroscopic data in Appendix A ($\Delta H^0_{298,r} - \Delta H^0_{0,r} = 0.3$ kJ mol^{-1}) giving $\Delta H^0_{0,r} = -2.8$ kJ mol^{-1} for the JANAF[38] database and +0.1 kJ mol^{-1} for Sandia.[1] A recent tabulation by Kerr[39] gives $\Delta H^0_{0,r} = +0.8$ kJ mol^{-1}. The differences reside primarily, although not exclusively, in

TABLE 6: Enthalpies of Formation of the Species Involved in Channels 1−7, for Sandia[1] and JANAF[38] Databases

	$\Delta H^0_{298,f}$/kJ mol^{-1}	
species	JANAF	Sandia
CH_3	145.7 ± 0.8	146.8
OH	39.0 ± 1.2	39.3
$^1CH_2$	424.0 ± 4.2	428.3
H_2O	-241.8 ± 0.04	−241.8
CH_3O		17.2
H	218.0 ± 0.006	218.0
CH_2OH		−17.6
HCHO	-155.9 ± 6.3	−108.6
H_2	0.0	0.0

$\Delta H^0_f(^1CH_2)$, and it is appropriate to examine the experimental and theoretical data on which this quantity is based, which are given in Table 7.

The majority of the data are based on photoionization or photodissociation measurements. The values for $CH_2(\tilde{X}^3B_1)$ and have been converted into heats of formation for the singlet state using the $T_0(\tilde{a}^1\ A_1)$ value of Jensen and Bunker.[40] The photodissociation measurements give the threshold for the singlet state directly. The most recent measurement, by Chen et al.,[41] gives the threshold to high accuracy (± 0.4 cm^{-1}), and the uncertainty given in Table 7 derives from that in the value for $\Delta H^0_{0,f}(CH_2CO)$ (44.8 ± 1.7 kJ mol^{-1}).[42] Doltsinis and Knowles[43] have recently performed high-level ab initio calculations, based on $^3CH_2 \rightarrow C(^3P) + H_2$ (see Table 7). The estimates of $\Delta H^0_{0,f}(^1CH_2)$ obtained in the present work are 428.0 and 429.4 kJ mol^{-1}, depending on the thermodynamic database used for the other radical species. The total uncertainty of ± 2.5 kJ mol^{-1} (2σ) includes the uncertainties in the other radical species as estimated in the JANAF tables. The agreement with the best spectroscopic data is excellent.

The threshold energy of channel 3 is a primary determinant of the competition between dissociation of CH_3OH^* to reform CH_3 + OH and its dissociation to generate $^1CH_2 + H_2O$. At high pressures, stabilization to form CH_3OH domains. Channel 3 becomes increasingly important as the pressure is decreased. The temperature dependence of the HDO yield obtained by Grotheer et al.[5,11,12] gives $\Delta H^0_{298,r} = 8 \pm 2$ kJ mol^{-1}, which, with the uncertainty of the measurements, corresponds also to their estimate for $\Delta H^0_{0,r}$. Their estimate, therefore, differs significantly from that reported here, which is based primarily on the work of Temps et al.[37] and of Hack et al.[35] Figure 5 plots $k_{1,3}(T)$ for $p = 1$ Torr based on our estimates and those of Grotheer et al.[5,11,12] The difference between them is substantial.

It should be noted that, since the ground state of OH has the term symbol $^2\Pi$, CH_3 + OH correlate with two triplet and two singlet CH_3OH surfaces. Were one of the triplet surfaces to be bound, it would provide a route through to $^3CH_2 + H_2O$. There is no information on such a low lying triplet state of CH_3 OH and this mechanism seems unlikely, given the unreactivity of $^3CH_2$ with species like H_2O. Recent ab initio calculations by Balint−Kurti[44] show a significant activation energy for this route from CH_3 + OH and a direct mechanism which does not involve a bound state of CH_3OH.

The present data are reasonably well fitted by the ME analysis with a fixed value of $\langle \Delta E \rangle_{down}$ (230 cm^{-1}), a negative temperature dependence in k_1^∞, and a $\Delta H^0_{0,3}$ value compatible with the Sandia database, i.e., an approximately thermoneutral channel 3. As discussed above, the overall rate constant is largely independent of pressure over the pressure range studied here. Figure 6 shows the microcanonical rate constants for the six dissociation channels as a function of energy. The only other significantly competing dissociation channel under the experimental conditions studied here is channel 7. The barrier height

TABLE 7: Experimental Measurements of $\Delta H^0_{0,f}(^1CH_2)$[a]

method	$\Delta H^0_{0,f}(^1CH_2)$/kJ mol^{-1}	ref
photoionization of CH_3 ($^3B_1$)	424.0 ± 4.2	Chupka and Lifshitz[51]
photoionization of CH_4, CH_2CO ($^3B_1$)	429.3 ± 1.7	McCulloh and Dibeler[52]
photodissociation threshold of CH_2CO ($^1A_1$)	425.5 ± 2.1	Lengel and Zare[53]
photodissociation threshold of CH_2CO ($^1A_1$)	426.3 ± 2.1	Feldmann et al.[54]
product energy distribution, 308 nm photolysis of CH_2CO ($^1A_1$)	429.3 ± 2.5	Hayden et al.[55]
photodissociation threshold of CH_2CO ($^1A_1$)	429.3 ± 1.7	Chen et al.[41]
activation energy for HDO production from CH_3OD ($^1A_1$)	434.2 ± 2.5	Grotheer et al.[5,11,12]
MRCI calculations on $^3CH_2 \rightarrow C(^3P) + H_2$ ($^3B_1$)	426.4 ± 1.0	Doltsinis and Knowles[43]
current estimate, using JANAF database[37] (for CH_3, OH, H_2O) and experimental value for $\Delta H^0_{0,r}$	428.0 ± 2.5	this work
current estimate, using SANDIA database[1] (for CH_3, OH, H_2O) and experimental value for $\Delta H^0_{0,r}$	429.4 ± 2.5	this work

[a] The estimate based on $^3B_1$ measurements have been converted into $\Delta H^0_{0,f}(^1CH_2)$ using the value of T_0ã^1 $A_1 = 37.65 \pm 0.06$ kJ mol^{-1} of Jensen and Bunker.[39]

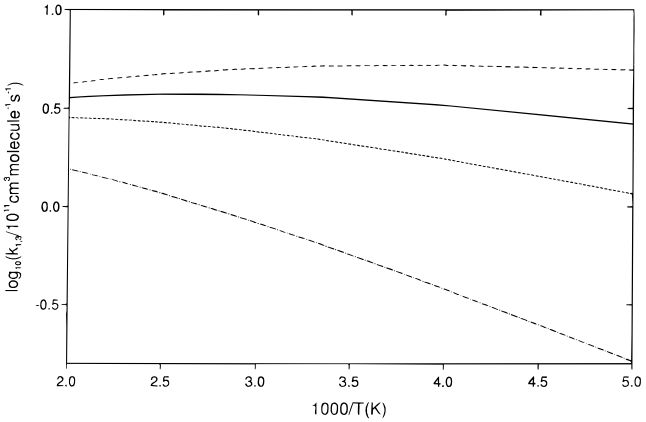

Figure 5. $k_{1,3}$ for $p = 1$ Torr based on the present estimates and those of Grotheer et al.[5,11,12] for different $\Delta H^{\ominus}_{0,3} - \Delta H^{\ominus}_{0,1}$. – –, −0.4 kJ mol^{-1} ; —, 1.6 kJ mol^{-1} ; ---, 3.6 kJ mol^{-1}; – • – • –, estimates of Grotheer et al.[5,11,12] (∼7.5 kJ mol^{-1}).

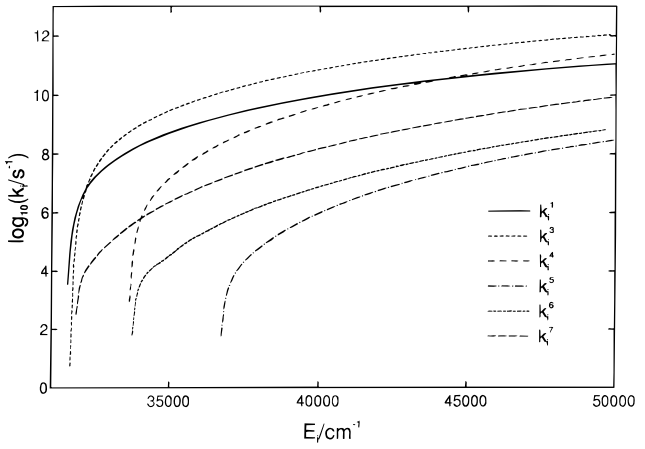

Figure 6. Micronanonical rate coefficients for each dissociation channel as a function of energy.

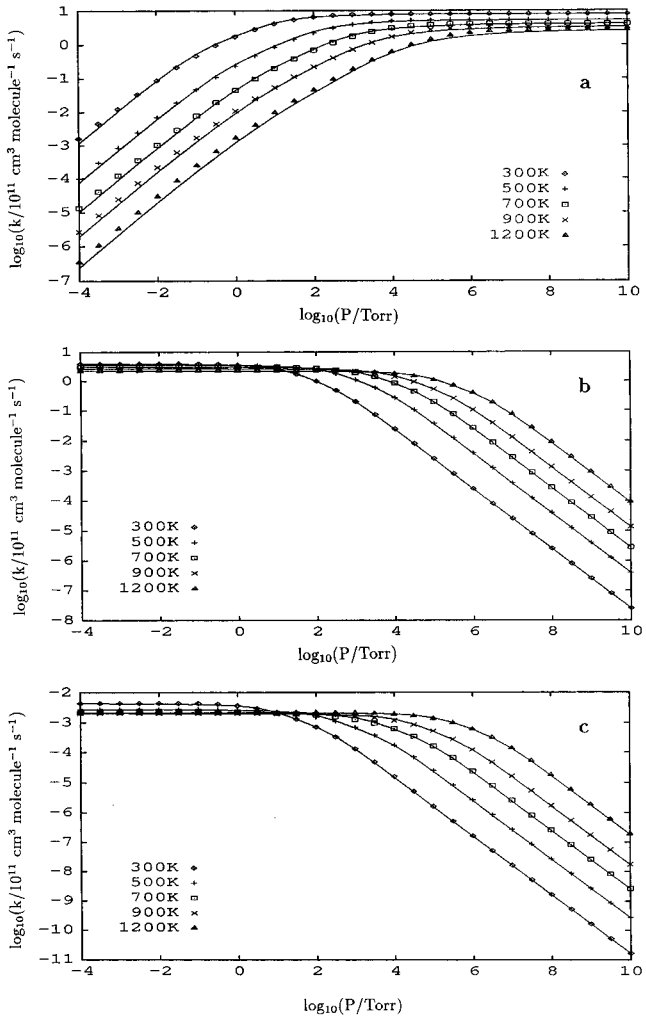

Figure 7. Pressure dependence of the rate coefficients for (a) channel 2, (b) channel 3 and (c) channel 7, as calculated from the master equation, for temperatures 300, 500, 700, 900, and 1200 K. Lines represent fittings based on the modified Troe formalism (see text).

chosen for this channel was taken from Harding's calculations.[2] Walch[34] gives a much lower value (355.6 kJ mol^{-1}) which leads to much greater prominence for this channel, such that it is not possible to reproduce the $^1CH_2$ yield observed by Temps et al.[37] Carstensen et al.[36] discussed this channel and could find no evidence for HCHO, which would be formed from HCOH by isomerization, supporting the higher transition state energy. Also the lower transition state energy predicts $k_{1,7} > k_{1,2}$ under the conditions studied by Oser et al.[5] at 300 and 480 K, which disagrees with the conclusion given by these workers that stabilization was the dominant channel at these temperatures. However, by examining their 700 K data,[11,12] an intermediate barrier height was required to fit the channel branching ratios obtained, i.e., $k_{1,7}/k_{1,2} \approx 5$ at 0.5 Torr.

Figure 7 shows plots of the canonical channel rate coefficients $k_{1,2}$, $k_{1,3}$ and $k_{1,7}$, against pressure for five temperatures. The rate coefficients for the other channels are independent of pressure, because the shape of the population density is governed almost exclusively by channels 1, 2, and 3. Channels 4 and 5 are strongly endothermic, and their temperature dependences are determined by the channel energies, given the assumptions made of temperature-independent association reactions. Figure 8 shows a plot of rate constants for channels 4−6 at 290 K. All

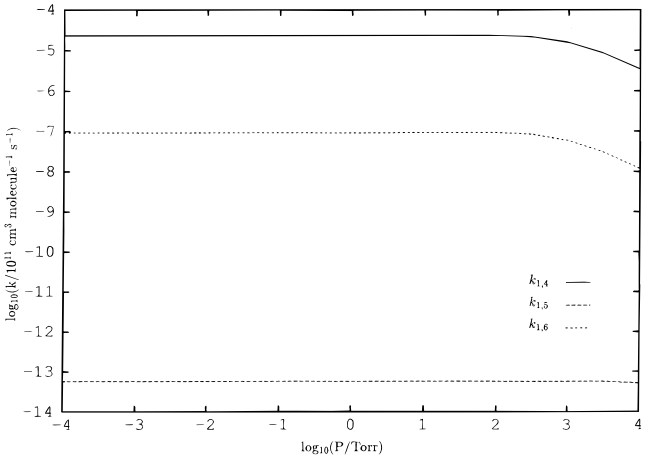

Figure 8. Pressure dependence of the rate coefficients for channels 4−6 as calculated from the master equation for 290 K.

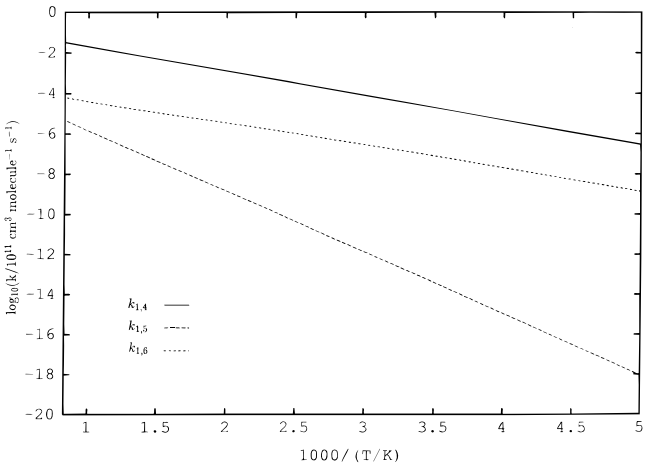

Figure 9. Arrhenius plots for channels 4−6 at $p = 1$ Torr.

are essentially independent of pressure. Figure 9 shows the Arrhenius plots for these channels, and the related Arrhenius forms are given in Appendix B. It should be noted that a potential limitation of ME calculation and fitting is the neglect of rotation, which can have differential effects on the channel rate constants because of differences in the shapes of the potential surfaces. While we have developed techniques for incorporating rotation into ME calculations,[56,57] such an approach in not feasible with a fitting routine based on the ILT.

The data generated from the master equation for channels 2, 3, and 7 with optimal parameters were fitted using the Troe formalism. The parameters for $k_{1,2}$ are given in Appendix B. In the latter two cases, however, modification of the basic formalism was required as indicated in ref 27. For channels 3 and 7, it is clear that the rate coefficient decreases as the pressure increases in contrast to the standard Lindemann type fall-off curve. The basic analytic form of the rate coefficient as a function of bath gas concentration was derived from the expression

$$\frac{1}{k} = \frac{1}{k^0} + \frac{[\mathrm{M}]}{k^\infty} \tag{31}$$

which has the correct limiting behavior at the extremes of the bath gas concentration [M]. Rearrangement of eq 29 leads to the following basic expression

$$\frac{k}{k^0} = \frac{1}{1 + P_\mathrm{r}} \tag{32}$$

where $P_\mathrm{r} = k^0[\mathrm{M}]/k^\infty$ is the reduced pressure and is analogous

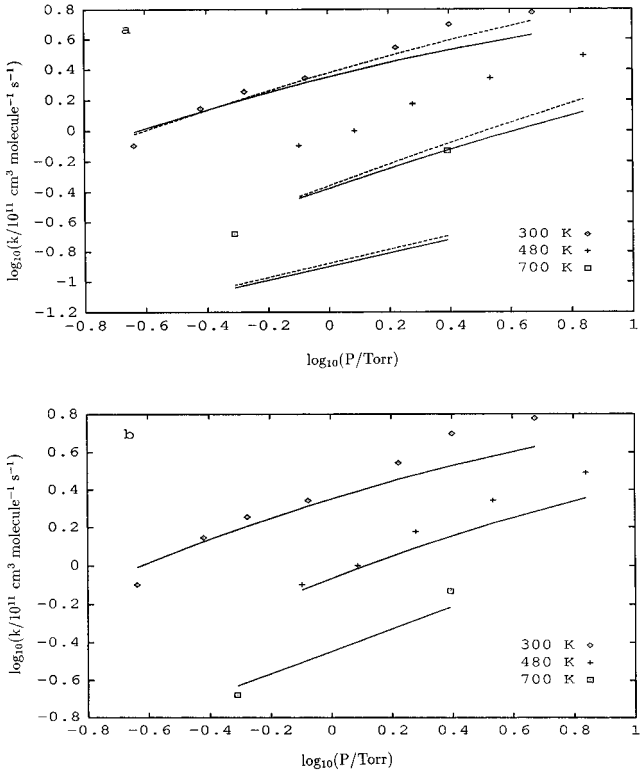

Figure 10. Experimental data of Oser et al.[5,11,12] (a) The full line indicates the fall-off obtained using parameters obtained from the data presented in this work. The broken line is the fit based on k_1^∞ obtained by Oser et al.[5] (b) Full lines indicate fall-off curves obtained using parameters obtained from the data presented in this work, with a modified $\langle \Delta E \rangle_{\mathrm{down}} = 230(T/300\ \mathrm{K})^{2.0}\ \mathrm{cm}^{-1}$.

to that that appears is the standard Lindemann−Hinshelwood factor. Equation 32 is corrected for broadening effects by applying a broadening factor $F(P_\mathrm{r})$, which is of exactly the same form as that used in the standard fall-off representation (see, for example, ref 29). The rate coefficients k_0 and k_∞ as well as F_{cent}, the parameter that governs the magnitude of the broadening factor, are all functions of temperature and were fitted to appropriate functional forms, the details of which are given in Appendix B.

The information content in the experimental data, is comparatively limited; the most important aspects are the pressure and temperature dependences. It is important, therefore, to compare the model results with literature data.

Oser et al.[5,11,12] obtained a strong pressure dependence in their measured rate constants, but they were "blind" to channel 3 (see section 1). Thus they were confined, according to the proposed model, to measurements of $k_{1,2}$ with very small contributions from channels 4−7. They fitted their data to obtain $k_1^\infty = 1.7 \times 10^{-10}$ cm^3 molecule^{-1} s^{-1}, independent of temperature. In an effort to understand the origin of this discrepancy, compared with our own measurements, the data reported by Oser et al.[5,11,12] were examined using the ME/ILT method of section 4, with the modification that channel 3 was excluded from the calculation. Figure 10a shows the data and fall-off curves calculated using the $k_1^\infty(T)$ obtained in the present experiments and that by Oser et al.[5] The fits are acceptable at 300 K but poorer for the other data. Although χ^2 is larger for our parameters, the fits are not significantly worse to the eye. The measurements of Oser et al.[5,11,12] were made far from the high-pressure limit so that quite a long extrapolation is needed. Figure 10b shows fall-off curves calculated using a temperature-dependent $\langle \Delta E \rangle_{\mathrm{down}} = 230(T/300\ \mathrm{K})^{2.0}\ \mathrm{cm}^{-1}$. Good agreement was obtained, though the parameters give very high values of $\langle \Delta E \rangle_{\mathrm{down}}$ at the higher temperatures. The higher

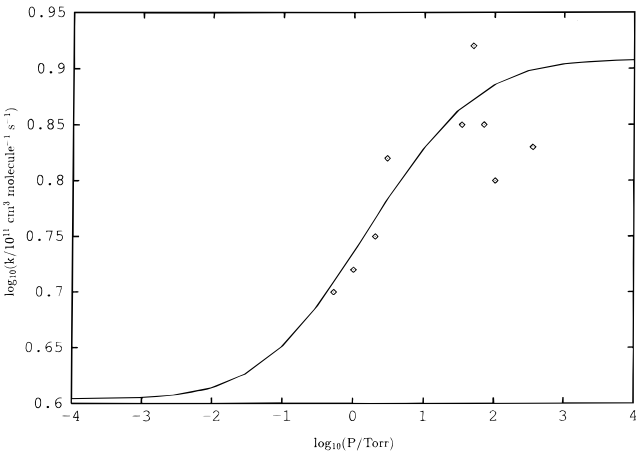

Figure 11. Experimental data of Temps et al.[37] and the calculated fall-off curve using the present ME model (eqs 29 and 30), for temperature 296 K.

pressure data reported here are largely insensitive to such a strong T dependence of $\langle\Delta E\rangle_{\text{down}}$. Figure 11 shows the data for k_1 measured by Temps et al.[37] and the fall-off curve calculated using the present ME model parameters (eqs 29 and 30). The agreement is excellent.

The data of Bott et al.[9] were examined using appropriate collisional parameters for the bath gas Ar and a $\langle\Delta E\rangle_{\text{down}}$ value of 400 cm^{-1}. The rate constant was calculated to be 2.3×10^{-11} cm^3 $molecule^{-1}$ s^{-1} at 1200 K and 760 Torr, which is within their experimental range, $(1.8 \pm 0.5) \times 10^{-11}$ cm^3 $molecule^{-1}$ s^{-1}. A comparison was also made with the data reported by Fagerström et al.[8] Rate coefficients for the various experimental conditions selected by these workers were calculated using the parameters given by equations 29 and 30. The bath gas used by Fagerström et al.[8] is SF_6, and so collision parameters appropriate for this gas were used together with a $\langle\Delta E\rangle_{\text{down}}$ value of 1000 cm^{-1}. The values obtained are shown in Table 5 together with the experimental values. Their values are consistently higher than our high-pressure limit of 8.0×10^{-11} cm^3 $molecule^{-1}$ s^{-1}.

7. Conclusions

The multichannel CH_3 + OH reaction system shows a complex temperature and pressure-dependent behavior. Table 1 and Figure 4 summarize the experimental data for CH_3 + OH in a helium diluent over the pressure range 7.6−678 Torr for the temperatures 290, 473, and 700 K. The reaction is largely pressure independent over the range studied. The experimental data were analyzed by a combined ME/ILT/RRKM procedure and the limiting high-pressure rate coefficient was obtained:

$$k_1^{\infty} = 8.0 \times 10^{-11} (T/300\ \text{K})^{-0.79}\ \text{cm}^3\ \text{molecule}^{-1}\ \text{s}^{-1} \qquad (33)$$

The threshold energy of the channel producing $^1CH_2$ and H_2O was estimated to be 379 ± 2 kJ mol^{-1}, which is about 1.6 kJ mol^{-1} higher than that of the entrance channel. At low pressures and/or high temperatures, channel 3 competes effectively with the stabilization channel, 2. Rate coefficients for channels 4−6 are essentially independent of pressure, and for channel 7 pressure-dependent rate coefficients were obtained. Representation of rate coefficients for each product channel are given in Appendix B. The parametric forms of the temperature and pressure-dependent rate coefficients for channels 2, 3, and 7 are based on the Troe formalism, while rate coefficients for channels 4−6 are expressed in Arrhenius form.

Acknowledgment. Discussions on certain technical aspects with Dr K. Hughes were most informative. We are grateful to Dr. G Balint-Kurti, Prof. T. Bérces, Dr. S. Dóbé, Dr. H-H Grotheer, Prof. P. Knowles, and Prof. F. Temps for continuing helpful discussions and for making results available prior to publication. This work was supported by the EPSRC through a postdoctoral fellowship (S.H.R.), by British Gas through a studentship to R.D.A.P. and through the EU through an HCM grant.

Appendix A

Molecular Parameters for ILT/RRKM/ME Analysis

CH_3OH. Vibrational frequencies/cm^{-1}: 3681, 2973(2), 2845, 1475, 1455, 1425, 1345, 1160, 1070, 1033, [270] (This frequency corresponds to internal rotation which was treated classically (see text)). Rotational constants/cm^{-1}: 4.259, 0.807, 5.25. Symmetry number (internal rotation): 3. $\Delta H^0_{f,0}$/kJ mol^{-1}: −212.42.

Channel 1. *CH_3.* Vibrational frequencies/cm^{-1}: 3162(2), 3044, 1396(2), 606. Rotational constants/cm^{-1}: 4.742 9.574. Symmetry number: 6. $\Delta H^0_{f,0}$/kJ mol^{-1} 135.23.

OH. Vibrational frequency/cm^{-1}: 3725.2. Rotational constant/cm^{-1}: 18.87. Spin−orbit splitting/cm^{-1}: 137. $\Delta H^0_{f,0}$/kJ mol^{-1}: 29.73.

Threshold energy[1] /kJ mol^{-1}: 377.4.

Channel 3. *$^1CH_2$.* Vibrational frequencies/cm^{-1}: 2865, 2806, 1353. Rotational constant/cm^{-1}: 20.142 9.1104(2). Symmetry number: 2. $\Delta H^0_{f,0}$/kJ mol^{-1}: 414.58.

H_2O. Vibrational frequencies/cm^{-1}: 3755.8, 3657.1, 1594.6 Rotational constant/cm^{-1}: 27.435, 12.062(2). Symmetry number: 2. $\Delta H^0_{f,0}$/kJ mol^{-1}: −251.67. Arrhenius parameters, A^{∞}, n^{∞}, E^{∞}, and T^{∞} : 1.6×10^{-10}, 0., 0., 1. Threshold energy/ kJ mol^{-1}: this study.

Channel 4. *CH_2OH.* Vibrational frequencies/cm^{-1}: 3650, 3019, 2915, 1459, 1334, 1183, 1048, 569. Rotational constants/cm^{-1}: 6.4364, 0.9884(2). Symmetry number: 2. $\Delta H^0_{f,0}$/kJ mol^{-1}: −28.95.

H. $\Delta H^0_{f,0}$/kJ mol^{-1}: 211.67. Arrhenius parameters, A^{∞}, n^{∞}, E^{∞}, and T^{∞}: 1.6×10^{-10}, 0., 0., 1. Threshold energy[1] /kJ mol^{-1}: 402.5.

Channel 5. *CH_3O.* Vibrational frequencies/cm^{-1}: 3320, 3311, 3216, 1657, 1599, 1582, 1159, 1064, 717.0. Rotational constants/cm^{-1}: 5.333, 0.867(2). Symmetry number: 3. $\Delta H^0_{f,0}$/kJ mol^{-1}: 5.9. Arrhenius parameters, A^{∞}, n^{∞}, E^{∞}, and T^{∞}: 1.31×10^{-11}, 0., 0., 1. Threshold energy[1] /kJ mol^{-1}: 439.3.

Channel 6. *CH_2O/H_2 Transition State.* Vibrational frequencies/cm^{-1} : 3195, 2295, 1740, 1574, 1429, 1369, 916, 3278, 1273, 1211, 1065. Rotational constants/cm^{-1}: 3.345, 0.944, 0.863 Symmetry number: 1. Threshold energy[2]/kJ mol^{-1}: 403.8.

Channel 7. *$HCOH/H_2$ Transition State.* Vibrational frequencies/cm^{-1}: 4130, 3199, 2323, 1564, 1498, 1347, 1291, 1122, 934, 622, 513. Rotational constants/cm^{-1}: 3.042, 0.839, 0.764. Symmetry number: 1 Threshold energy[2]/kJ mol^{-1}: 380.8.

Collision Parameters. $\sigma[CH_3OH]$ = 3.626 Å; σ[He] = 2.551 Å; $\epsilon[CH_3OH]$ = 481.8 K; ϵ[He] = 10.22 K.

Appendix B

This appendix gives the formulae used to fit the rate data for channels 2, 3, and 7, and Arrhenius parameters for channels 4−6 for temperature 200 K ≤ T ≤ 1200 K.

Parameters for the fall-off curves for channel 2:

$$k^0 = 4.4 \times 10^{-26}(T/300)^{-6.21} \times \exp(-671/T)\ \mathrm{cm^6\ molecule^{-2}\ s^{-1}}$$

$$k^\infty = 8.0 \times 10^{-11}(T/300)^{-0.79}\ \mathrm{cm^3\ molecule^{-1}\ s^{-1}}$$

$$F_{\mathrm{cent}} = -0.756\exp(-70.7/T) + \exp(-T/5646)$$

Parameters for the fall-off curves for channel 3:

$$k^0 = 1.0 \times 10^{-10}(T/300)^{-0.91} \times \exp(-275/T)\ \mathrm{cm^3\ molecule^{-1}\ s^{-1}}$$

$$k^\infty = 1.5 \times 10^{7}(T/300)^{5.8}\exp(485/T)^{-1}$$

$$F_{\mathrm{cent}} = 0.664\exp(-T/3569) + 0.336\exp(-T/108) + \exp(-3240/T)$$

Parameters for the fall-off curves for channel 7:

$$k^0 = 1.9 \times 10^{-14}(T/300)^{-0.12} \times \exp(209/T)\ \mathrm{cm^3\ molecule^{-1}\ s^{-1}}$$

$$k^\infty = 7.5 \times 10^{2}(T/300)^{8.0}\exp(1240/T)\ \mathrm{s^{-1}}$$

$$F_{\mathrm{cent}} = 0.295\exp(-T/3704) + 0.705\exp(-T/312) + \exp(-1238/T)$$

Arrhenius parameters for channels 4−6:

$$k_4(T) = 1.2 \times 10^{-12}\exp(-2760/T)\ \mathrm{cm^3\ molecule^{-1}\ s^{-1}}$$

$$k_5(T) = 2.0 \times 10^{-14}\exp(-6990/T)\ \mathrm{cm^3\ molecule^{-1}\ s^{-1}}$$

$$k_6(T) = 5.3 \times 10^{-15}\exp(-2530/T)\ \mathrm{cm^3\ molecule^{-1}\ s^{-1}}$$

References and Notes

(1) Lee, R. J.; Ripley, F. M.; Miller, J. A. *Chemkin Thermodynamic Data Base*. SANDIA Report 87-8215 UC4; Sandia National Laboratories: Livermore, CA, 1987.

(2) Harding, L. B.; Schlegel, H. B.; Krishnan, R.; Pople, A. J. *J. Phys. Chem.* **1980**, *84*, 3394.

(3) Dean, A. M.; Westmoreland, P. R. *Int. J. Chem. Kinet.* **1987**, *19*, 207.

(4) Green, N. J. B; Pereira, R. A.; Pilling, M. J.; Robertson, S. H. Twenty Third Symposium (International) on Combustion, 1990.

(5) Oser, H.; Stothard, N. D.; Humpfer, R.; Grotheer H.-H. Just, T. Twenty Fourth Symposium (International) on Combustion, Orleans, France, 1992, 597.

(6) Hochanadel, C. J.; Sworski, T. J.; Orgen, P. J. *J. Phys. Chem.* **1980**, *84*, 129.

(7) Anastasi, C.; Ellermann, P.; Pagsberg, P.; Polak, S. *J. Chem. Soc. Faraday Trans.* **1991**, *87*, 2991.

(8) Fagerström, K.; Lund, A.; Mahmoud, G.; Jadkowski, J. T.; Ratajczak, E. *Chem. Phys. Lett.*, **1993**, *206*, 226.

(9) Laszlo, B.; Dóbé, S.; Bérces T.; Marta, F. Twelfth International Symposium on Gas Kinetics, 1992.

(10) Bott, J. F.; Cohen, N. *Int. J. Chem. Kinet.* **1991**, *23*, 1017.

(11) Humpfer, R.; Oser, H.; Grotheer, H.-H.; Just, T. Twenty Fifth Symposium (International) on Combustion, 1994, 721.

(12) Humpfer, R.; Oser, H.; Grotheer, H. H. *Int. J. Chem. Kinet.* **1995**, *27* (6), 577.

(13) Hughes, K. J.; Pereira, R. A.; Pilling, M. J. *Ber. Bunsen-Ges. Phys. Chem.* **1992**, *92*, 1352.

(14) Jordan, M. J. T.; Smith, S.C.; Gilbert, R. G. *J. Phys. Chem.* **1991**, *95*, 8685.

(15) Brouard, M.; Macpherson, M.T.; Pilling M. J. *J. Phys. Chem.* **1989**, *93*, 4047.

(16) Lightfoot, P. D.; Kirwan, S. P.; Pilling, M. J. *J. Phys. Chem.* **1988**, *92*, 4938.

(17) Macpherson, M. T.; Pilling M. J.; Smith, M. J. C. *J. Phys. Chem.* **1985**, *89*, 2268.

(18) Press, W. H.; Flannery, B. P.; Teukolsky, S. A.; Vettering, W. T. *Numerical Recipes*; Cambridge University Press: Cambridge, U.K., 1988.

(19) Quack, M. Private communication.

(20) Ashfold, M. N. R. Private communication.

(21) Cvetanović, R. J.; Singleton, D. L.; Paraskevopoulos, G. *J. Phys. Chem.* **1979**, *83*, 50.

(22) Tulloch, J. M.; Macpherson, M. T.; Morgan, C. A.; Pilling, M. J. *J. Phys. Chem.* **1982**, *86*, 3812.

(23) Wallington, T. J.; Kurylo, M. J. *J. Chem. Phys.* **1987**, *91*, 5050.

(24) Troe, J. *J. Phys. Chem.* **1979**, *83*, 114.

(25) Troe, J. *Ber. Bunsen-Ges. Phys. Chem.* **1983**, *87*, 161.

(26) Gilbert, R. G.; Luther, K.; Troe, J. *Ber. Bunsenges. Phys. Chem.* **1983**, *87*, 169.

(27) Larson, C. W.; Patrick, R.; Golden, D. M. *Combust. Flame* **1984**, *58*, 229.

(28) Robertson, S. H.; Pilling, M. J.; Baulch, D. L.; Green, N. J. B. *J. Phys. Chem.* **1995**, *99*, 13452.

(29) Holbrook K. A; Pilling, M. J.; Robertson, S. H. *Unimolecular Reactions*; (Wiley: New York, 1996.

(30) Beyer, T.; Swinehart, D. F. *Commun. Assoc. Comput. Machin.* **1973**, *16*, 379.

(31) Stein, S. E.; Rabinovitch, B. S. *J. Chem. Phys.* **1973**, *58*, 2438.

(32) Seakins, P. W.; Robertson, S. H.; Pilling, M. J.; Slagle, I. R.; Gmurczyk, G. W.; Bencsura, A; Gutman, D.; Tsang, W. *J. Phys. Chem.* **1993**, *97*, 4450.

(33) Davies, J. W.; Green N. J. B.; Pilling, M. J. *Chem. Phys. Lett.* **1986**, *126*, 373.

(34) Walch, S. P. *J. Chem. Phys.* **1993**, *98*, 3163.

(35) Hack, W.; Wagner, H. Gg.; Wilms, A. *Ber. Bunsen-Ges. Phys. Chem.* **1988**, *92*, 620.

(36) Carstensen, H.-H.; Wagner, H. Gg. *Ber. Bunsen-Ges. Phys. Chem.* **1995**, *99*, 1539.

(37) Deters, R.; Otting, M.; Wagner, H. Gg.; Temps, F.; László, B.; Dóbé, S.; Bérces, T; Márta, F. *Ber. Bunsen-Ges. Phys. Chem.*, in press.

(38) Chase, M. W., Jr.; Davies, C. A.; Downey, J. R., Jr.; Frurip, D. J.; McDonald, R. A.; Syverud, A. N. In *JANAF Thermochemical Tables*, 3rd ed. *J. Phys. Chem. Ref. Data* 1985, *14* (Suppl. 1).

(39) Kerr, J. A. In *Strength of Chemical Bonds, Handbook of Chemistry and Physics*, 77th ed.; Lide, D. R., Ed.; CRC Press: Boca Raton, FL, 1996; pp 9−51.

(40) Bunker, P. R.; Jensen, Per; Kraemer, W. P.; Beardsworth, R. *J. Chem. Phys.* **1986**, *85*, 3724.

(41) Chen, I.-Chia; William, H; Green, Jr.; Moore, C. B. *J. Chem. Phys.* **1988**, *89*, 314.

(42) Nuttal, R. L.; Laufer, A. H.; Kilday, M. V. *J. Chem. Thermodyn.* **1971**, *3*, 167.

(43) Doltsinis, N. L.; Knowles, P. E. *J. Chem. Soc., Faraday Trans.*, in press.

(44) Balint-Kurti; private communication.

(45) Baulch, D. L.; Cobos, C. J.; Cox, R. A.; Esser, C.; Franck, P.; Just, Th; Kerr, J. A.; Pilling, M. J.; Troe, J.; Walker, R. W.; Warnatz, J. *J. Chem. Phys. Ref. Data* **1992**, *21*, 441.

(46) Braun, W.; Bass, A .M.; Pilling, M.J. *J. Chem. Phys.* **1970**, *52*, 5131.

(47) Tsang, W.; Hampson, R. F. *J. Phys. Chem. Ref. Data* **1987**, *15*.

(48) Zellner, R.; Erler, K.; Field, D. Sixteenth Symposium (International) on Combustion **1977**, 939.

(49) Heinemann-Fiedler, F.; Hoyermann, K. *Ber. Bunsen-Ges. Phys. Chem.* **1988**, *92*, 1472.

(50) Hoyermann, K.; Loftfield, N.S.; Sievert, R.; Wagner, H. Gg. Eighteenth Symposium (Internatinoal) on Combustion 1981, 831.

(51) Chupka, W. A.; Lifshitz, C. *J. Chem. Phys.* **1968**, *48*, 1109.

(52) McCulloh, K. E.; Dibeler, V. H. *J. Chem. Phys.* **1976**, *64*, 4445.

(53) Lengel, R. K.; Zare, R. N. *J. Am. Chem. Soc.* **1978**, *100*, 7495.

(54) Feldmann, D; Meier, K.; Zacharias, H; Welge, K. H. *Chem. Phys. Lett.* **1978**, *59*, 171.

(55) Hayden, C. C.; Neumark, D. M.; Shobatake, K.; Sparks, R. K.; Lee, Y. T. *J. Chem. Phys.* **1982**, *76*, 3607.

(56) Robertson, S. H.; Pilling, M. J.; Green, N. J. B. *Mol. Phys.* **1996**, *89*, 1531.

(57) Robertson, S. H.; Pilling, M. J.; Gates, K. E.; Smith, S. C. *J. Comput. Chem.* **1997**, *18*, 1004.